RADIANT ABSORPTION CHARACTERISTICS OF CORRUGATED CURVED TUBES

by

Milan Lj. DJORDJEVIĆ[a,*], Velimir P. STEFANOVIĆ[b], Dragan V. KALABA[a], Marko V. MANČIĆ[b], and Marko D. KATINIĆ[c]

[a] Faculty of Technical Sciences, University of Pristina, Kosovska Mitrovica, Serbia
[b] Faculty of Mechanical Engineering, University of Nis, Nis, Serbia
[c] College of Slavonski Brod, Slavonski Brod, Croatia

Original scientific paper
https://doi.org/10.2298/TSCI160420263D

The utilization of modern paraboloidal concentrators for conversion of solar radiation into heat energy requires the development and implementation of compact and efficient heat absorbers. Accurate estimation of geometry influence on absorption characteristics of receiver tubes is an important step in this process. This paper deals with absorption characteristics of heat absorber made of spirally coiled tubes with transverse circular corrugations. Detailed 3-D surface-to-surface Hemicube method was applied to compare radiation performances of corrugated and smooth curved tubes. The numerical results were obtained by varying the tube curvature ratio and incident radiant heat flux intensity. The details of absorption efficiency of corrugated tubes and the effect of curvature on absorption properties for both corrugated and smooth tubes were presented. The results may have significance to further analysis of highly efficient heat absorbers exposed to concentrated radiant heating.

Key words: *heat absorbers, corrugated tubes, spiral coil, absorption efficiency*

Introduction

The utilization of modern paraboloidal concentrators for conversion of solar radiation into heat energy requires the development and implementation of compact and efficient heat absorbers (HA). Knowledge of the distribution of radiant heat flux incident upon the absorber tubes at any point along their length and circumference will aid in developing meaningful heat transfer information for the absorber. The objective of this paper was to investigate the absorption characteristics of spirally coiled tubes with transverse circular corrugations.

Ali and Hanoaka [1] investigated the use of a V-corrugated plate as an absorber in a solar air collector and pointed out that corrugations enhance the convective heat transfer coefficient and at the same time the effective convective heat transfer area increases, resulting in a collective increase of the convective conductance. Sparrow and Lin [2] stated that the V-corrugated plate absorber provides an apparent absorptivity to the incident radiation flux of almost unity even when painted with commercial black paint. On the other hand, the absorptive and flow characteristics of corrugated absorber tubes could significantly differ

* Corresponding author, email: milan.djordjevic@pr.ac.rs

from those of investigated plate geometry. Pressure drop and stability of flow in straight and curved pipes with transverse circular corrugations have already been investigated [3], but information about absorption characteristics of corrugated tubes exposed to radiant heat flux could not be find in literature.

The radiant heat flux field is incident on only one-half of the circumference of the absorber tubes in parabolic dish receivers, so that the outer surface of the tube could be split along the tube axis into two symmetric segments. In further analysis only the segment exposed to radiant heat flux will be considered. Classical analysis technique employing analytical models is applicable to very few, relatively simple geometry configurations and cases. In this case a numerical technique was adopted, since a useful model requires capability for using the concept of radiosity in complex geometry (curved surfaces). Heat transfer models used to quantify theoretical predictions are usually based on Monte Carlo ray tracing [4] and finite-volume techniques [5].

Geometric and numerical model

Transversely corrugated Archimedean spiral coil is innovative design solution of HA. The Archimedean spiral with the pitch approximately equal to the maximum outer diameter of the corrugated tube was selected between different types of spirals in order to achieve the most favorable ratio of active surface area and the total volume of the HA. Geometrical parameters of analyzed sinusoidal corrugated tube and Archimedean spiral coil are shown in tab. 1.

Table 1. Geometrical parameters of tested configurations

Transversely corrugated straight tube				Transversely corrugated Archimedean spiral coil			
d	9.3	mm	Minimum internal diameter	R_{min}	25	mm	Minimum radius of the coil
d_0	11.7	mm	Maximum internal diameter	R_{max}	202	mm	Maximum radius of the coil
d_e	12.2	mm	Maximum external diameter	n	13	–	Number of coil turns
s	0.25	mm	Wall thickness	L	9.324	m	Length of the coil
e	1.2	mm	Corrugation depth	p_s	13.6	mm	Spiral coil pitch
p_c	4.2	mm	Corrugation pitch				

Numerical simulations in ANSYS Fluent 15 based on finite volume method were carried out to compare absorption characteristics of straight and coiled transversally corrugated tubes with different curvature ratio $\delta = d_e /2R$, where d_e is maximum external diameter of corrugated tube and R is radius of curvature. For this particular case, average curvature ratio varies from 0.031 (corresponding to 1st or outermost spiral turn) to 0.192 (corresponding to 13th or innermost spiral turn).

The effects of the corrugations on absorption properties can only be benchmarked if compared with a smooth tube, and therefore results for a smooth tube were also presented in this paper. The external diameter of comparative smooth tube was chosen to be equal to maximum external diameter of corrugated tube in order to make possible to construct a smooth Archimedean spiral coil with identical geometrical parameters to that made of corrugated tube.

The tubes in the numerical simulations were exposed to the heat fluxes in the range 10^4-$1.5\cdot10^5$ W/m^2. One Sun, as the amount of power flux, represents the solar irradiance in

the form of electromagnetic radiation in the wide wavelength range and is taken to be 1000 W/m^2. Less than 60% of this value can be converted into heat, which means that for the considered range of heat fluxes reaching the surface of the absorber appropriate paraboloidal (dish) concentrator should have concentration ratio approximately in range 20-270. Concentration ratio values in stated range are typical for modern paraboloid concentrators that are applicable in low and middle temperature systems.

The solar receiver prototype consists of a cylindrical cavity containing a black-painted transversely corrugated Archimedean spiral coil that absorbs radiant heat flux. An ideal 3-D computational model should be build upon credible physical model that includes concentrator and receiver, what demands tremendous computational resources. Since the optical characteristics of concentrator were not of interest in this study, it was assumed that radiant heat flux on the focal plane is uniform. On the other hand, for the purpose of achieving high precision, the numerical model would not contain the whole spiral, but only much smaller segments of the spiral, whose lengths were equal to the length of four corrugation periods. Those segments were curved with different curvature ratios to represent geometrical parameters of different spiral coil turns, fig. 1.

Previous assumptions allowed modeling radiant energy exchange between surfaces within enclosure, what significantly simplified computational model. Cuboid enclosure with dimensions 0.2 × 0.2 × 0.1 m was selected for computational domain, where the hot lower surface (0.2 × 0.2 m) and the colder upper surface (0.2 × 0.2 m) were included in the radiation heat transfer, while the sidewalls were excluded from the process. The gap between the surfaces was filled with air, but the flow equations were not solved and the media was treated as a stationary object. Tube segments, whose absorption characteristics were investigated, were placed in the center of the upper surface, fig. 2. Dimensions of enclosure surfaces that exchange radiant energy were set in order to obtain central area of upper surface (where the distribution of radiant heat flux is uniform) much bigger than the dimensions of tested segments. Moreover, three identical segments were always placed in that area in order to take into account influence of neighboring absorber tubes. The mutual irradiation by the adjacent tubes has nominally the same temperature for the emitter and absorber, what justifies the gray body enclosure model assumption that the emissivity equals the absorptivity ($\varepsilon = \alpha$). Later numerical experiments showed that mutual irradiation by the adjacent tubes increases the intensity of the incident radiation on the outer surface of the absorber tubes up to 5.3%. All the presented results in further analysis were related to the central tube segment of described geometric model.

Figure 1. Tested segments of Archimedean spiral coil

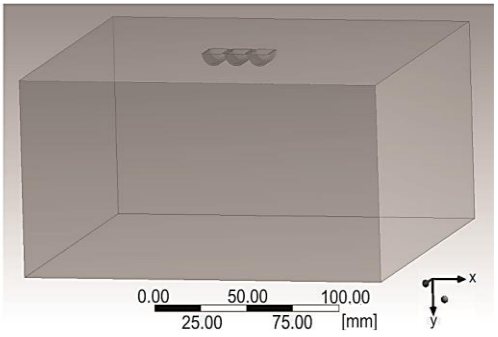

Figure 2. Geometric model of cuboid enclosure

The radiant heat absorption in the absorber (opaque metal material) is volumetric phenomena in reality. However, most of the absorption in the absorber occurs very close to the surface (about 6Å) [6]. Therefore, the error in treating radiant energy absorption as a surface phenomenon should be relatively small [7].

Thermal radiation is a very complex phenomenon and although the governing equations are well known, they are difficult to solve. This difficulty is due to radiation intensity as a function of position, direction, wavelength and temperature. In some cases these dependencies are not straightforward. Radiation analysis of enclosures becomes very complicated unless some simplifying assumptions are made. It is common to assume the surfaces of an enclosure to be opaque, diffuse and gray. Also, each surface of the enclosure is isothermal [8].

The various numerical methods have been used to solve the radiative transfer equation. All these methods have their advantages and disadvantages, and no one is considered as the best one for all applications. In the present work the surface-to-surface (S2S) radiation model was used. The energy flux leaving a given surface is composed of directly emitted and reflected energy. The reflected energy flux is dependent on the incident energy flux from the surroundings, which then can be expressed in terms of the energy flux leaving all other surfaces.

The S2S radiation model presents a method to obtain the radiative intensity field for radiation exchange in an enclosure of gray-diffuse surfaces. The main assumption of the S2S model is that any absorption, emission or scattering of radiation by medium between surfaces can be ignored and only S2S radiation need to be considered for analysis.

The energy exchange between two surfaces depends on their size, separation distance and orientation. These parameters are accounted for by a geometric function called a view factor. The amount of incident energy upon a surface from another surface is a direct function of the S2S view factor F_{jk}. The incident energy flux $q_{in,k}$ can be expressed in terms of the energy flux leaving all other surfaces:

$$A_k q_{in,k} = \sum_{j=1}^{N} A_j q_{out,j} F_{jk} \tag{1}$$

where A_k is the area of surface k, F_{jk} – the view factor between surface k, and surface j and N are the number of surfaces.

The energy flux leaving a given surface is composed of directly emitted and reflected energy. The reflected energy flux is dependent on the incident energy flux from the surroundings, which then can be expressed in terms of the energy flux leaving all other surfaces. The following equation was used for the energy reflected from surface k:

$$q_{out,k} = \varepsilon_k \sigma T^4 + \rho_k q_{in,k} \tag{2}$$

where $q_{out,k}$ is the energy flux leaving the surface, ε_k – the emissivity, σ – the Stefan-Boltzmann constant, and $q_{in,k}$ – the energy flux incident on the surface from the surroundings.

In another form of the aforementioned equation, the radiosity, J, can be utilized. The total energy given off a surface k is given by:

$$J_k = E_k + \rho \sum_{j=1}^{N} F_{kj} J_j \tag{3}$$

where E_k represents the emissive power of surface k. The view factor between two finite surfaces j and k is given by:

$$F_{jk} = \frac{1}{A_j} \int_{A_j} \int_{A_k} \frac{\cos\theta_j \cos\theta_k}{\pi r^2} \delta_{jk} \mathrm{d}A_j \mathrm{d}A_k \tag{4}$$

where δ_{jk} is determined by the visibility of $\mathrm{d}A_k$ to $\mathrm{d}A_j$ ($\delta_{jk} = 1$ if $\mathrm{d}A_k$ is visible to $\mathrm{d}A_k$, and 0 otherwise).

The emissivity and absorptivity of a gray surface are independent of the wavelength. Also, by Kirchoff's law [9], the emissivity equals the absorptivity ($\varepsilon = \alpha$). For a diffuse surface, the reflectivity is independent of the outgoing or incoming directions. In this work, the gray-diffuse model was used and the model assumes that if a certain amount of radiant energy, E, is incident on a surface, a fraction, ρE, is reflected, a fraction, αE, is absorbed, and a fraction, τE, is transmitted. For most applications the surfaces in question are opaque to thermal radiation. Fluent, the CFD code used in this investigation, also assumes surfaces to be opaque. The transmissivity, therefore, can be neglected. From conservation of energy follows that $\alpha + \rho = 1$ (since $\varepsilon = \alpha$) and $\rho = 1 - \varepsilon$.

The S2S radiation model is very expensive in terms of computation effort and memory requirements when there are a large number of radiating surfaces. The number of radiating surfaces can be reduced by grouping faces together to form surface clusters. Detailed information concerning S2S could be found in literature [10, 11].

Fluent provides two methods for computing view factors, the Hemicube and the Ray tracing method. The Hemicube method uses a differential area-to-area method and calculates the view factors on a row by-row basis. The view factors calculated from the differential areas are summed to provide the view factor for the whole surface. This method originated from the use of the radiosity approach in the field of computer graphics [12]. The Hemicube method is based upon three assumptions about the geometry of the surfaces: aliasing, visibility, and proximity [10].

While the Hemicube method projects radiating surfaces onto a hemicube, the Ray tracing method instead traces rays through the centers of every hemicube face to determine which surfaces are visible through that face. Both methods were tested during this study. Obtained values of surface incident radiation are very close, except that the values obtained by Hemicube method are slightly higher, as a rule. Deviations were not greater than 1‰. All results presented in further analysis were obtained by using the Hemicube method.

In all numerical runs the emissivity of the enclosure upper surface and surfaces of tubes were set to 0.9, what could be achieved in practice by using commercially available absorptive paints (Pyromark 2500, [13]). The emissivity of the enclosure lower surface was set to 1.

Volume cells of hybrid mesh were generated in the computational domain as following: structured mesh on surfaces of enclosure, especially fine on tube segments surfaces, and unstructured in volume of enclosure to limit the total number of elements. A careful check for the grid-independence of the numerical solution has been made to ensure the accuracy of the numerical scheme. Numerical calculations indicated that the value of curvature ratio, δ, and rate of radiation heat transfer are the most critical for the radiation model validation, because the largest discrepancies from analytical data were obtained for the highest rate of radiation heat transfer. Hence, the integrated incident heat flux over the corrugated segment of the 13th coil turn ($\delta_{av} = 0.192$) have been used to test the independency of the calculation results from the applied grids (results are reported in tab. 2). The intensity of incident heat flux that the corrugated segment had been exposed was 150000 W/m^2 (the intensity of incident heat flux on central area of upper enclosure surface where the tested tube segments were placed).

The calculations have been carried out on four different grids and the relative error of the control quantity was calculated. Boundary conditions for the grid-independence tests were formulated as follows: temperature and emissivity of the hot lower enclosure surface T_h = 1,486 K and ε_h = 1, temperature and emissivity of the corrugated tube segment and the upper enclosure surface T_c = 423 K and ε_c = 0.9.

Table 2. Relative errors of the integrated incident heat flux over the corrugated segment of the 13th coil turn (δ_{av} = 0.192)

	Number of cells			
	(I) 669449	(II) 775009	(III) 908793	(IV) 1136923
Integrated incident heat flux, [W]	33.516	33.506	33.486	33.479
Relative error of integrated incident heat flux, [%]	0.11	0.08	0.02	–

Although the magnitudes of relative error are relatively small for all grids tested, it was concluded that grid resolution larger than 9×10^5 cells (case III, second finest grid) in the studied enclosure geometries would be enough to produce results independent from the applied numerical grid.

A series of calculations were performed to investigate the validity of numerical computations. The analytical and computed data for the net rate of radiation heat transfer between hotter (surface 1) and colder surface (surface 2) of enclosure (tube segments were excluded) together with their relative differences are shown in tab. 3. Analytical solution, as well as numerical, assumes that the surfaces are isothermal and diffuse emitters and reflectors and that the surfaces are separated by a nonparticipating medium (air) (eq. 5):

$$\dot{Q}_{12} = \frac{\sigma\left(T_1^4 - T_2^4\right)}{\frac{1-\varepsilon_1}{A_1\varepsilon_1} + \frac{1}{A_1 F_{12}} + \frac{1-\varepsilon_2}{A_2\varepsilon_2}} \tag{5}$$

where F_{12} = 0.425 for this particular case (view factor between two aligned parallel rectangles of equal size). In all validation cases the temperature of upper enclosure surface was kept constant (423 K), while the temperature of lower enclosure surface was varied, tab. 3.

Figure 3 shows that the computed and analytical solutions almost overlap each other and the computed results are well within the acceptable range with a maximum deviation less than 2.5%. It also could be noted that deviation increases with increasing rates of radiation heat transfer.

The results of the grid-independence tests, tab. 2, guarantee accuracy of numerical results. Since no relevant data, neither experimental nor numerical, about radiant absorption characteristics of corrugated curved tubes could be found in literature, validity of numerical computations is obtained by comparing numerical and analytical results for flat surface (analytical results are available only for simple geometries), and those results were presented

Table 3. Validation of numerical S2S model

The net rate of radiation heat transfer, [W]	Temperature of hotter surface, [K]			
	755	1130	1345	1486
Analytical solution	269.61	1471.28	2982.72	4458.69
Numerical solution	264.51	1436.76	2911.21	4351.05
Deviation, [%]	1.89	2.35	2.4	2.41

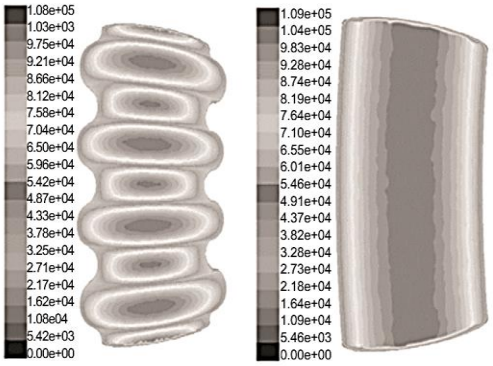

Figure 3. Distribution of the surface incident radiation (d_e / 2R = 0.084; q_p = 100000 W/m^2) (*for color image see journal web site*)

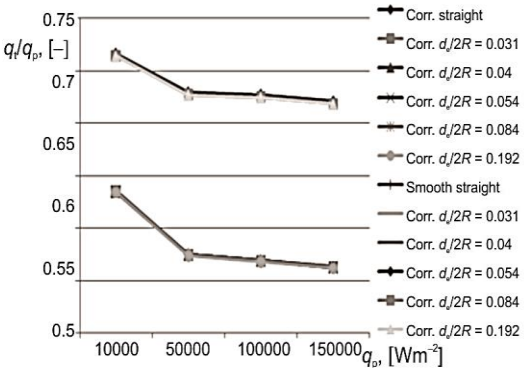

Figure 4. The effect of geometry on area-weighted average incident heat flux (*for color image see journal web site*)

in tab. 3. Accordingly, it can be regarded that numerical results for the cases of corrugated and smooth curved tubes would not deviate significantly from those for flat surfaces. Thus, errors of presented numerical results could be approximated with deviation values obtained within displayed validation study.

In all simulations the temperature of upper enclosure surface and tested tube segments was kept constant (423 K), while the temperature of lower enclosure surface was varied. In this way different intensities of uniform incident heat flux were obtained on central area of upper surface (where tube segments were placed). Simulated intensities of incident heat flux on planar surface were 10000, 50000, 100000, and 150000 W/m^2.

Tested segments of the both transversally corrugated and smooth tube spiral coil, whose lengths were equal to the length of four corrugation periods, were central parts of the 1st, 4th, 7th, 10th, and 13th turn of the considered Archimedean spiral coil. Curvature ratios, δ, of those segments were 0.0313, 0.04, 0.0538, 0.084, and 0.192, respectively. Besides the curved segments, the straight segments of the same length were tested too, making a total of 12 geometry configurations.

Each of 12 geometry configurations, fig. 1, were tested with four different rates of incident heat flux, which meant that results of 48 simulations were used for analysis.

Results and discussion

Since only half of the perimeter of the spirally coiled tubes of heat absorber can see the radiation source, there will always be a variation of incident flux around the circumference of the tube. The energy absorbed by the surface is a function of the tubes projected area normal to the radiation vector. The incident heat flux on the outer surface of the tubes was obtained from the calculation of the intensity of the incident radiation on the tubes. Example of the incident radiation distribution on the outer surface of the tubes whose curvature ratio equals 0.084 was shown in fig. 3 (incident heat flux on planar surface was 100000 W/m^2). It is obvious that the intensity of the incident radiation reaching the surface of tubes is not uniform, with the maximum at the tube crowns, declining to relatively low values at the tube tangent positions.

The ratio of the area-weighted average surface incident heat flux on tested tube sections, q_t, to the incident heat flux on planar surface qp was plotted against q_p, fig. 4. It is

obvious that smooth wall tube offers better absorptive performance compared to sinusoidal corrugated wall tube with equal maximum external diameter. Curvature ratio has small influence on absorptive characteristics, since all lines in diagram collapse to two lines, each one representing characteristics for corrugated and smooth tubes separately. Incident heat flux affects the absorption characteristics of either corrugated or smooth tube only at lower intensities. With the increase of incident heat flux intensity the absorption capacity initially degrades and reaches almost constant value for higher incident heat flux intensities.

The effects of the corrugations on absorptive properties can only be benchmarked properly if the increment in total absorptive surface of corrugated tubes over smooth tubes is taken into account. In order to achieve that, the surface incident heat flux was integrated over surface to give the absorbed power. The ratio of absorbed power of corrugated tube, I_{cw}, to the absorbed power of smooth tube, I_{sw}, was plotted against incident heat flux q_p, fig. 5. This ratio could be regarded as geometry-dependent absorptive efficiency of corrugated tubes.

Incident heat flux intensity decisively influences absorption efficiency. The absorption efficiency and incident heat flux intensity are inversely proportional, with strong negative relationship at the beginning of observed interval (10000-50000 W/m^2). Absorption efficiency remains almost constant for higher values of incident heat flux. Curvature ratio has a little influence on absorption efficiency of corrugated tubes, but could be noticed that the inner turns of spiral coil have slightly higher absorption efficiency than the outer turns and straight tube.

The effect of curvature on absorption properties for both corrugated and smooth wall tubes is shown in fig. 6. The ratio of absorbed power of coiled tube, I_c, to the absorbed power of straight tube, I_s, was plotted against curvature ratio, δ.

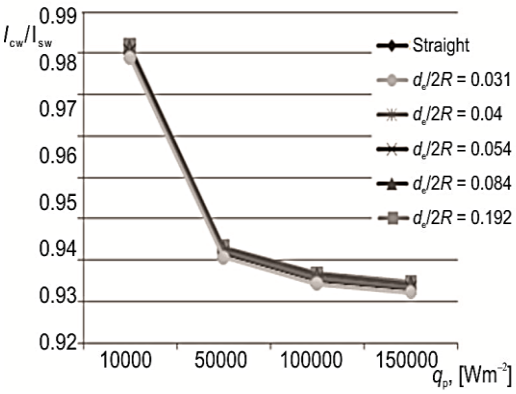

Figure 5. The ratio of absorbed power of corrugated tube to absorbed power of smooth tube

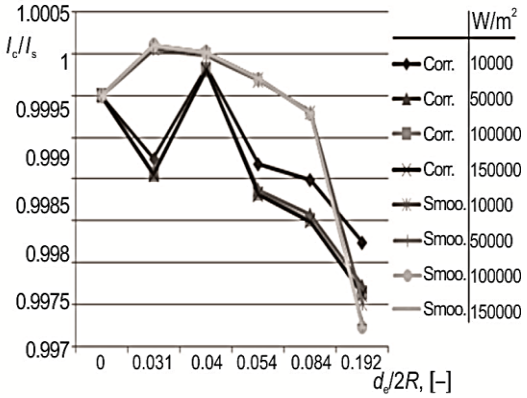

Figure 6. The effect of curvature on absorption properties

Results imply that absorbed power on curved smooth tube increases for small curvature ratios, reaches its maximum, and then decreases, especially for high curvature ratios. On the other hand, the behavior of corrugated tubes is rather interesting. Namely, absorbed power on curved corrugated tube decreases with the increase of curvature ratio, then suddenly reaches its maximum for a certain curvature ratio, and subsequently continues to decrease as curvature ratio grows further. These findings could be important for geometry

optimization of coiled corrugated and smooth wall tube absorbers with fixed curvature ratio (helical absorbers).

Conclusions

Results of 48 numerical simulations were used for estimation of absorption properties of curved corrugated and smooth tubes exposed to radiant heat flux. Based on the results presented and discussed here, one can conclude the following:

- Smooth wall tube offers slightly better absorption performance compared to sinusoidal corrugated wall tube with equal maximum external diameter. This does not necessarily have to represent a significant shortcoming, since the hydraulic and thermal conditions of flow within pipes decisively influence the overall performance of heat absorber.
- The influence of incident heat flux intensity on absorption efficiency of either corrugated or smooth tubes is much more pronounced that the influence of curvature.
- From the point of absorption efficiency, the optimal coil curvature ratios were determined for both corrugated and smooth tubes. This has implications for development of highly efficient HA with fixed curvature ratio (helical absorbers).

Acknowledgment

The support of the Ministry of Education, Science and Technological Development of the Republic of Serbia through projects 42006 is gratefully acknowledged.

Nomenclature

A_k – area of surface k, [m^2]
E_k – emissive power of surface k, [Wm^{-2}]
F_{jk} – surface-to-surface view factor between two finite surfaces j and k, [–]
I_c – absorbed power of coiled tube, [W]
I_{cw} – absorbed power of corrugated tube, [W]
I_s – absorbed power of straight tube, [W]
I_{sw} – absorbed power of smooth tube, [W]
J – radiosity, [Wm^{-2}]
N – number of surfaces, [–]
$\dot{Q}_{12}$ – net rate of radiation heat transfer between surfaces, [W]
$q_{in,k}$ – incident energy flux on surface k, [Wm^{-2}]
$q_{out,k}$ – energy flux leaving the surface k, [Wm^{-2}]
q_p – incident heat flux on planar surface, [Wm^{-2}]
q_t – area-weighted average incident heat flux on tube surface, [Wm^{-2}]
T – temperature, [K]

Greek symbols

α – absorptivity, [–]
δ – curvature ratio (= d_e /2R), [–]
δ_{ij} – Kronecker delta, [–]
ε – emissivity, [–]
ρ – reflectivity, [–]
σ – Stefan-Boltzmann constant, [Wm^{-2}K^{-4}]
τ – transmissivity, [–]

References

[1] Ali, A., Hanaoka, Y., Experimental Study on Laminar Flow Forced-Convection in a Channel with Upper V-Corrugated Plate Heated by Radiation, *International Journal of Heat and Mass Transfer, 45* (2002), 10, pp. 2107-2117
[2] Sparrow, E., Lin, S., Absorption of Thermal Radiation in a V-Groove Cavity, *International Journal of Heat and Mass Transfer, 5* (1962), 11, pp. 1111-1115
[3] Djordjević, M., *et al*., Pressure Drop and Stability of Flow in Archimedean Spiral Tube with Transverse Corrugations, *Thermal Science, 20* (2016), 2, pp. 579-591
[4] Shuai, Y., *et al*., Radiation Performance of Dish Solar Concentrator/Cavity Receiver Systems, *Solar Energy, 82* (2008), 1, pp. 13-21
[5] Cheng, Z. D., *et al*., Numerical Simulation of a Parabolic trough Solar Collector with Nonuniform Solar Flux Conditions by Coupling FVM and MCRT Method, *Solar Energy, 86* (2012), 6, pp.1770-1784

[6] Incropera, F., DeWitt, D., *Fundamentals of Heat and Mass Transfer*, John Wiley and Sons, New York, USA, 1990
[7] Forristall, R., Heat Transfer Analysis and Modeling of a Parabolic trough Solar Receiver Implemented in Engineering Equation Solver, Technical Report NREL/TP-550-34169, NREL, Golden, Col., USA, 2003
[8] Nouanegue, H., *et al*., Conjugate Heat Transfer by Natural Convection, Conduction and Radiation in Open Cavities, *International Journal of Heat and Mass Transfer, 51* (2008), 25-26, pp. 6054-6062
[9] Rohsenow, W. M, *et al*., *Handbook of Heat Transfer*, McGraw-Hill Handbooks, New York, USA, 1998
[10] ***, ANSYS FLUENT Theory Guide, Release 15.0, ANSYS Inc., Canonsburg, Penn, USA, 2013
[11] ***, ANSYS FLUENT User's Guide, Release 15.0, ANSYS Inc., Canonsburg, Penn., USA, 2013
[12] Cohen, M. F., Greenberg, D. P., The Hemi-Cube: A Radiosity Solution for Complex Environments, *Computer Graphics, 19* (1985), 3, pp. 31-40
[13] Ho, C. K., *et al*., Characterization of Pyromark 2500 for High-Temperature Solar Receivers, *Proceedings*, 6th International Conference on Energy Sustainability of ASME, San Diego, Cal., USA, 2012, pp. 509-518

Paper submitted: April 20, 2016
Paper revised: October 28, 2016
Paper accepted: October 31, 2016